Forming Anisotropic Crystal Composites: Assessing the Mechanical Translation of Gel Network Anisotropy to Calcite Crystal Form

Palin, D.; Style, Robert W.; Zlopaša, Jure; Petrozzini, Jonathan J.; Pfeifer, Mark A.; Jonkers, H.M.; Dufresne, Eric R.; Estroff, Lara A.

DOI
10.1021/jacs.0c12326

Publication date
2021

Document Version
Accepted author manuscript

Published in
Journal of the American Chemical Society

Citation (APA)
Palin, D., Style, R. W., Zlopaša, J., Petrozzini, J. J., Pfeifer, M. A., Jonkers, H. M., Dufresne, E. R., & Estroff, L. A. (2021). Forming Anisotropic Crystal Composites: Assessing the Mechanical Translation of Gel Network Anisotropy to Calcite Crystal Form. *Journal of the American Chemical Society*, *143*(9), 3439-3447. https://doi.org/10.1021/jacs.0c12326

Forming Anisotropic Crystal Composites: Assessing the Mechanical Translation of Gel Network Anisotropy to Calcite Crystal Form

Damian Palin, Robert W. Style, Jure Zlopaša, Jonathan J. Petrozzini, Mark A. Pfeifer, Henk M. Jonkers, Eric R. Dufresne, and Lara A. Estroff*

KEYWORDS: Crystal growth, affine deformation, mechanical confinement, fracture mechanics, biomineralization.

ABSTRACT: The promise of crystal composites with direction-specific properties is an attractive prospect for diverse applications, however, synthetic strategies for realizing such composites remain elusive. Here, we demonstrate that anisotropic agarose gel networks can mechanically "mold" calcite crystal growth, yielding anisotropically-structured, single-crystal composites. Drying and rehydration of agarose gel films result in the affine deformation of their fibrous networks to yield fiber alignment perpendicular to the drying plane. Precipitation of calcium carbonate within these anisotropic networks results in the formation of calcite crystal composite discs oriented parallel to the fibers. The morphology of the discs, revealed by nano-computed tomography imaging, evolves with time and can be described by linear-elastic fracture mechanics theory, which depends on the ratio between the length of the crystal and the elasto-adhesive length of the gel. Precipitation of calcite in uniaxially deformed agarose gel cylinders results in the formation of rice-grain shaped crystals, suggesting the broad applicability of the approach. These results demonstrate how the anisotropy of compliant networks can translate into desired crystal composite morphologies. This work highlights the important role organic matrices can play in mechanically "molding" biominerals and provides an exciting platform for fabricating crystal composites with direction-specific and emergent functional properties.

INTRODUCTION

Anisotropy is a key feature of biomineralized tissues.[1-4] The formation of these tissues is intimately associated with anisotropically-structured, organic, extracellular matrices. These matrices provide a structural scaffold and source of chemical functionality that mechanically "molds" and chemically modulates the inorganic mineral phase into anisotropic forms (e.g., nanoscale platelets and rods).[1,2,4-7] The resulting biomineralized tissues display outstanding direction-specific, mechanical,[2,8] and optical[5,9,10] properties. Understanding the role anisotropic organic networks play in directing crystal formation can, therefore, provide insights into biomineral formation and strategies for the design and synthesis of anisotropic crystal composites with direction-specific and emergent functional properties.

The question of how biology controls crystal habit has puzzled scientists for centuries.[11,12] The Dutch zoologist Pieter Harting was perhaps the first scientist to try to answer this question, growing calcareous crystals in the blood and bile of chopped up oysters.[11] Since this seminal work, scientists have pieced together parts of the puzzle, providing insights into the origins of biologically-controlled crystal habit. Early experiments demonstrated how inorganic and organic additives can influence the habit of crystals grown in solution.[13-15] Later experiments showed how chemically-functionalized two-dimensional (2D) templates can direct nucleation and dictate the orientation of crystals grown in a solution;[16-18] and how growth within rigid three-dimensional (3D) templates can control crystal morphology[19,20] and polymorph selectivity.[21]

Inspired by the mineralized organic matrices used by organisms, crystal growth in gels has emerged as a powerful synthetic platform for understanding and modeling biogenic crystal formation.[22] Gels provide a diffusion-limited environment, which can be used to control crystal habit.[22-26] Calcite crystals grown in agarose gels, for example, can have morphologies ranging from equilibrium rhombohedra to hopper-like or skeletal-shaped structures.[22,25] The formation of hopper-like crystals is attributed to diffusion dominated growth conditions in the absence of convective currents, which results in stable, spherical concentration contours surrounding polyhedral crystals.[27] These crystals, thus, experience different ion concentrations at different locations, and grow faster at their vertices than their centers, leading to the characteristic hopper morphology with concave faces and exaggerated vertices. Gel studies, as with the solution studies described above, have also shown that crystal habit can be controlled within gels via the addition of inorganic and organic additives;[24,28,29] and in the presence of chemically-functionalized 2D templates.[30] Further, chemical functionality covalently linked to the gels can interact with growing crystals modifying their habit,[29,31-33] which can, in turn, be modulated by mechanically deforming the gels.[31,33]

Multiple studies have demonstrated that when various crystals are grown in different gels, they can occlude the gel network, leading to the formation of a wide range of crystal-gel composites,[22,25,34-41] including protein-agarose,[34] calcite-agarose,[22,25,35,37,39] calcite-xyloglucan,[36] hematite-silica,[38] C_{60}-poly[2-methoxy-5-(2-ethylhexyloxy)-1,4-phenylenvinylene][40] and iron oxide-metal coordinate polymer[41] composites. By growing crystals with intrinsic functional properties[38,40,41] and using gels doped with functional nanoparticles (which can become occluded within the crystals),[36,37,39] the resulting crystal composites were endowed with magnetic,[36,37] optical,[36,37,39] photocatalytic,[38] and optoelectronic[40] properties. Further, by growing calcite crystals in agarose, a hydrophilic,

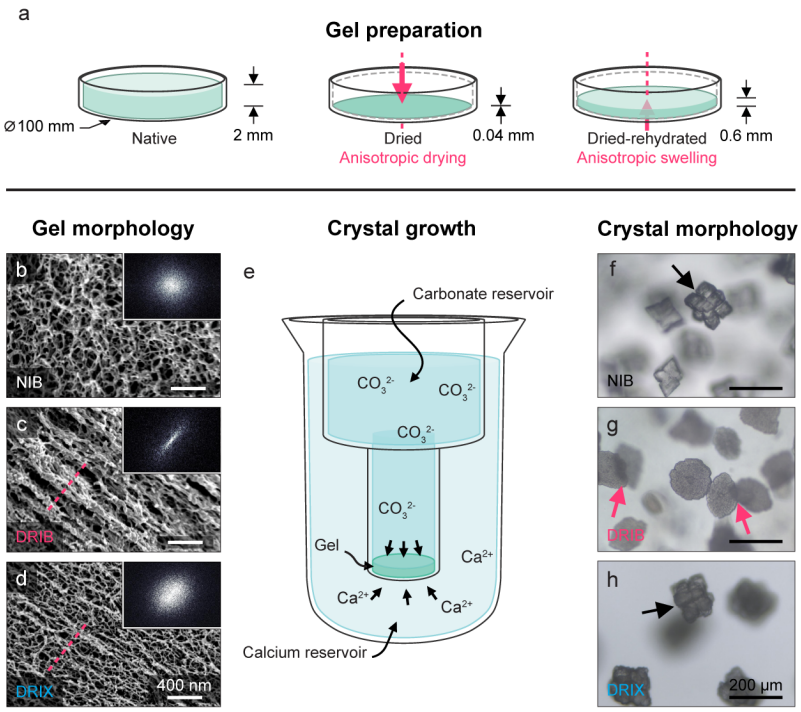

Figure 1. a) A schematic illustration of the drying-rehydration approach used to produce anisotropically-structured agarose gel films. The pink arrows indicating the drying direction (a, center) and swelling direction (a, right). b-d) Representative scanning electron microscope (SEM) images showing the microstructure of: b) a native agarose IB gel (3 w/v%; NIB) film; c) an agarose IB film after drying and rehydration (DRIB); and d) a dried-rehydrated agarose IX gel (3 w/v%; DRIX) film, all following critical point drying, and cryo-fracturing. Insets: Corresponding fast Fourier transforms (FFTs) of the images, produced using MATLAB R2018b (MathWorks). e) A schematic of the solution-based double-diffusion setup used to precipitate calcium carbonate crystals in the agarose films. f-h) Light microscope images of the crystallites formed in: f) a NIB gel; g) a DRIB gel; and h) a DRIX gel, after 4 weeks diffusion (50 mM $CaCl_2$ and $NaHCO_3$). a-d) The pink dashed lines in (c,d) run perpendicular to the drying plane (i.e., parallel to the drying direction), the black arrows in (f,h) point to crystals with hopper-like morphologies and the pink arrows in (g) to overlapping thin, disc-like crystals.

uncharged gel, researchers have been able to assess the mechanical occlusion of gel networks into growing crystals.[22,25] In one study,[25] the authors demonstrated that gel occlusion results from a competition between the strength of the gel network and the crystallization pressure exerted by a growing crystal, which depends on the supersaturation of the solution;[42,43] and that there is a critical gel strength and crystal growth rate at which this occlusion occurs. Although these studies have shed light on the mechanical role of gels in modulating crystal growth, the structure of these gels has been decidedly isotropic. Interesting questions, therefore, arise: *What would happen if we introduced structural anisotropy into a compliant, uncharged gel? Would this structure translate to a rigid crystal; if so, by what mechanism; and could this translation be controlled?* To answer these questions, we have developed a strategy for shaping crystal composites in anisotropically-structured gels. We chose the well-established model crystal-gel pair, calcite and agarose, to demonstrate the feasibility of this approach. We examine both the structuring of the agarose gels and shape formation of calcite crystals within the agarose and propose a physical model to describe the translation of gel anisotropy into crystal form.

EXPERIMENTAL DESIGN

To investigate the mechanical influence of anisotropic networks on crystal habit, we selected agarose IB as a hydrophilic and uncharged biopolymer that assembles to form a fibrous gel. Given that highly ordered gel/clay composite films can be formed via a straightforward drying process,[44] we decided to use a similar approach to anisotropically structure agarose IB. Briefly, we: 1) cast native gel (3 w/v%, NIB) films (Figure 1a, left); 2) dried the NIB films overnight in air forming free-standing dried (DIB) films, which maintained their diameter and reduced dramatically in thickness (Figure 1a, center); and 3) rehydrated the DIB films with deionized (DI) water to form dried-rehydrated (DRIB) films, which again maintained their diameter and this time increased in thickness, but not to the original thickness of the NIB films (Figure 1a, right). We analyzed the swelling behavior of the films using a combination of scanning electron microscopy (SEM) to visualize the nano-to-microscale structure, two-dimensional X-ray diffraction (2D-XRD) to quantify the degree of fiber orientation, and mechanical testing to determine the modulus and work to fracture. We grew crystals in the films via solution-based double diffusion (50 mM $CaCl_2$ and $NaHCO_3$, Figure 1e). We monitored the crystals' habit and morphology via light microscopy, their morphology via SEM, their morphology and orientation within the gel via nano-computed tomography (nanoCT), and crystal phase via Raman spectroscopy. To better understand the mechanical effect of the DRIB gels over crystal habit, we also grew crystals in NIB gel films, isotropically-structured Agarose IB gels, and dried-rehydrated Agarose IX (3 w/v%, DRIX) gel films, anisotropically-structured low strength gels (Agarose IX is over ten times weaker than agarose IB[25]). These films and the

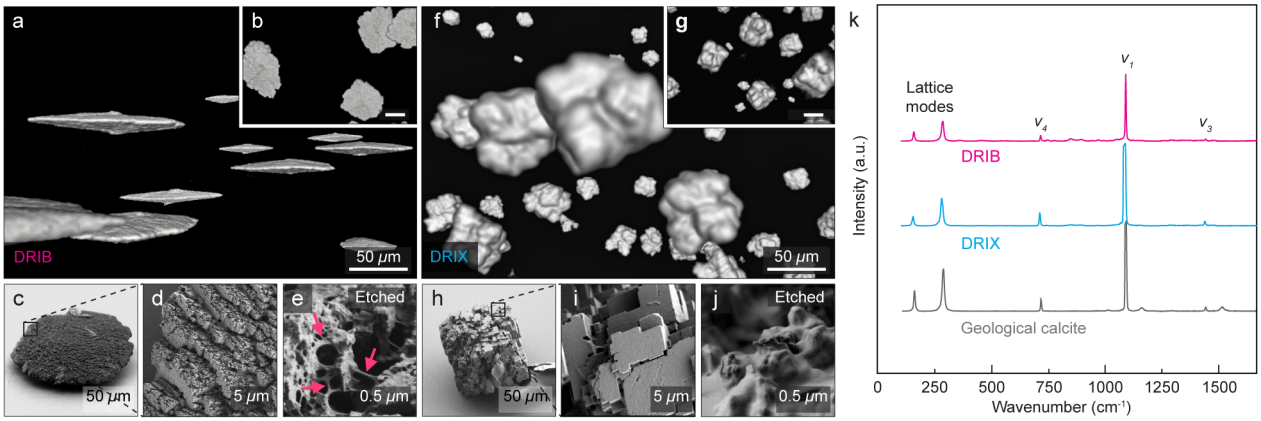

Figure 3. a-e) Images of crystals formed in a dried-rehydrated agarose IB gel (3 w/v%, DRIB); and f-j) crystals formed in a dried-rehydrated agarose IX gel (3 w/v%, DRIX) film, after 4 weeks diffusion (50 mM $CaCl_2$ and $NaHCO_3$). a,b,f,g) Reconstructed nano-computed tomography (nanoCT) data showing (a,f) an overview and (b,g) a plan view, of the crystals. The white volumes correspond to the mineral phase and black to agarose. The scale bars in (b,g) are 50 μm. c-e,h-j) SEM images showing: (c,h) overviews of individual crystals and (d,i) the surface of the same crystals at higher magnifications, and (e,j) crystals at high magnifications after etching in deionized water for 4 days. The pink arrows in (e) point to polymer bundles running through the crystals. k) Representative Raman spectra of crystals formed in a DRIB and DRIX film and of geological calcite.

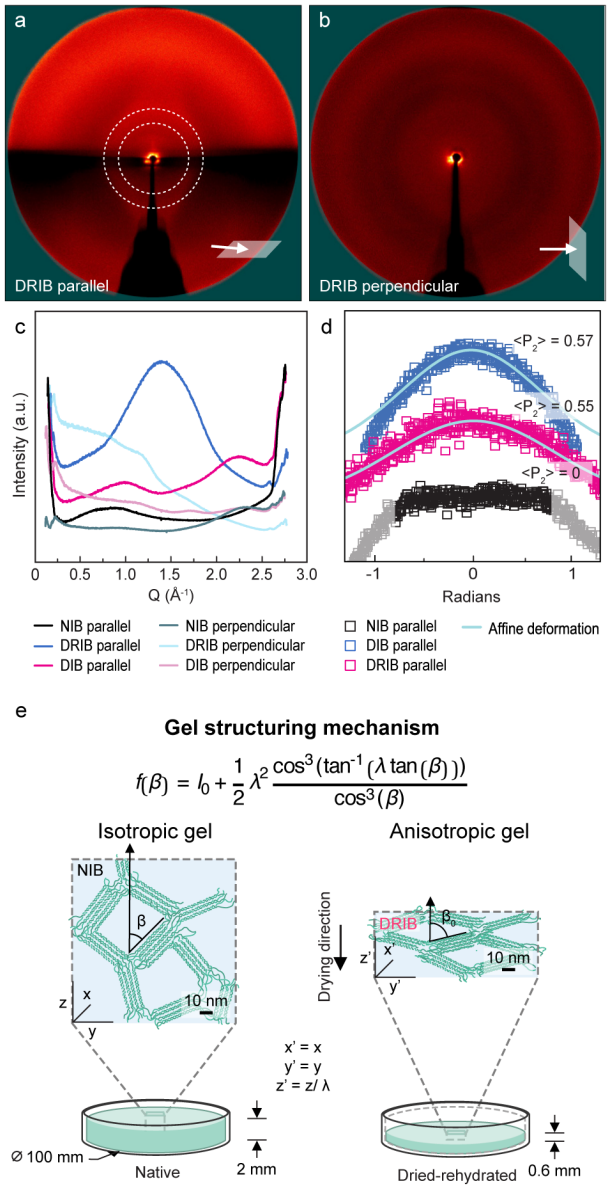

Figure 2. a,b) 2D x-ray diffraction patterns of a dried-rehydrated agarose IB (3 w/v%; DRIB) gel film taken with the incident beam a) at a grazing angle (2.2°) and b) perpendicular to the drying plane. c) Radial plots and d) azimuthal intensity profiles generated from the 2D scattering images taken parallel to the films. In (d), the azimuthal intensity profile for NIB gel was integrated over a Q of 0.5-1 A^{-1}, the DIB over 0.75-1.25 A^{-1}, and the DRIB over 1-1.75 A^{-1}, and fitted with the modified affine deformation model (MADM), equation in (e).[44] The square symbols represent the X-ray data and the solid lines the fits. Based on the MADM, the order parameter <P_2> was calculated for the DIB film as 0.57 and the DRIB film as 0.55, and for the NIB films as an isotropic gel is 0. The X-ray data for the NIB films beyond -0.8 and 0.8 radians is noise and grayed. e) A schematic depicting the affine deformation of the agarose IB films resulting from the drying-rehydration process. The dashed white circles in (a) represent the integration limits for the azimuthal intensity profile in (d).

crystals formed in them were analyzed, much like those formed in the DRIB gels.

RESULTS AND DISCUSSION

Gel Structure and Properties. Stereomicroscope images of the agarose IB and IX films show that they are macroscopically plastically deformed due to the drying-rehydration process (going from 100 × 2 mm to 100 × 0.6 mm, Figures 1a and S1). SEM images of the agarose IB gels show that this deformation persists down to the microscopic scale, as their network structure remodels from an isotropic network of pores (~50 nm) and nanofiber bundles (~20 nm in diameter, Figure 1b) to an anisotropic network of pores (~100 × 20 nm) and fiber bundles (~20 nm in diameter, Figure 1c). SEM images of the DRIX films show that they are an anisotropic network of smaller pores (~50 × 10 nm) and nanofiber bundles (~10 nm in diameter, Figure 1d). Fast Fourier transforms (FFTs) of the SEM images confirm the orientation of the gel networks (Figure 1b,c,d, inset). 2D-XRD analysis of the DIB and DRIB films confirms their anisotropic structure at the molecular scale (Figure 2a-d, S2c-f). When the incident beam passes perpendicularly through the surface of the films (i.e., parallel to the drying direction), an isotropic diffraction ring appears at ~1 A^{-1}, d ≈ 0.7 nm (Figure 2b and S2b,d,f), which is consistent with the spacing between

adjacent agarose chains.[45] When the film orientation is changed so that the beam is in a grazing configuration parallel to the surface of the film (i.e., perpendicular to the drying direction), this ring becomes two meridional crescents indicating that the films have an anisotropic network structure (Figure 2a and S2a,c,e).

Crystal Characteristics. Light microscope analysis of the crystals formed in the NIB gel (mechanically strong, isotropically structured) and DRIX gel (mechanically weak, anisotopically structured) films have hopper-like rhombohedral morphologies (Figure 1f,h, S3a-f) and the crystals formed in the DRIB gel (mechanically strong, anisotropically structured) films have thin, disc-like morphologies aligned perpendicular to the drying direction of the films, as it is possible to see through crystals above to crystals below when they overlap (Figures 1g (pink arrows), S3g-l). Given that hopper-like morphologies are known to form in NIB gels,[25] we did not analyze these crystals further. SEM and nanoCT imaging of the crystals formed in the DRIB films confirmed that they are discs aligned parallel to the drying plane of these films (Figures 3a-b, S4i-l) and that the crystals formed in the DRIX films are hoppers with no preferential alignment within these gels (Figures 3f-g, S4m-p). Higher magnification images of the surface structures of individual discs and hoppers reveal highly aligned {104} facets of calcite (Figure 3c,d,h,i, and S6). When comparing among discs, however, there appears to be no consistent orientation of the calcite facets with respect to the flattened face of the discs (Figure S6). In other words, the calcite lattice does not have a preferred orientation with respect to the discs. Raman spectroscopy confirms that the discs and hoppers are calcite (Figure 3k). The discs, despite their non-equilibrium morphology, surprisingly, demonstrate single crystal-like character, "blinking" when viewed through crossed-polarizers (Figure S3). Similar to previous reports of calcite grown in agarose,[22,25] gentle etching of the discs reveals that they are composites with agarose bundles running throughout their interior (Figures 3e, S5a,b). In contrast, when the hoppers are etched (Figures 3j and S5c,d), no occluded gel fibers are revealed, rather a thin polymer sheet appears to cover the surface of the crystals.

Affine Deformation of Gels. The formation of the discs in the DRIB films versus the formation of the hoppers in the NIB and DRIX films indicates that the anisotropic structure of the DRIB films is important for disc formation. But *how does this structure come about?* To better understand the origins of the anisotropic network structure in DRIB gels, we investigated whether this structuring could be described by affine deformation.[44,46] Affine deformation assumes that the local strain in a material is uniform and equivalent to the global macroscopic strain. If in our case the gel films are affinely deformed, then the orientation of the fiber network, as measured by 2D-XRD, should be predictable using a modified affine deformation model (MADM):[44] $f(\beta) = I_0 + \frac{1}{2}\lambda^2 \frac{\cos^3(\tan^{-1}(\lambda \tan(\beta)))}{\cos^3(\beta)}$ where I_0 is the baseline intensity of the azimuthal intensity profile, and β is the azimuthal angle, from the diffraction patterns, and λ is the degree of vertical film compression. The order parameter $\langle P_2 \rangle$ of the film's structure can be calculated according to $\langle P_2 \rangle = \frac{\int_{-1}^{1} P_2(\cos\beta) f(\beta) \mathrm{d}\cos(\beta)}{\int_{-1}^{1} f(\beta) \mathrm{d}\cos(\beta)}$ where $P_2(\cos(\beta))$ is a second-order Legendre polynomial of $\cos(\beta)$: $P_2(\cos(\beta)) = \frac{1}{2}(3\cos^2(\beta) - 1)$. For a perfectly anisotropic material $\langle P_2 \rangle = 1$ and a perfectly isotropic material $\langle P_2 \rangle = 0$. The MADM model describes the azimuthal intensity profiles of the DIB and DRIB films well (Efron's pseudo-R^2 of 0.66 and 0.64, respectively, Figure 2d). The in-plane order parameters for the DIB and DRIB films were similar ($\langle P_2 \rangle$ = 0.57 and $\langle P_2 \rangle$ = 0.55, respectively), and higher than that of the isotropic NIB films ($\langle P_2 \rangle = 0$). These results indicate that the films are affinely deformed as a result of drying and that this deformation is maintained after rehydration (Figure 2e). The drying causes the polymer chains/bundles of the gel to "concertina down" on themselves, resulting in the macroscopic deformation of the gel (Figure S1a,c) and their nanoscale anisotropic structure (Figure S2c). Rehydration of the films causes them to partially reswell (Figure S1e), resulting in their anisotropic fissured nanoscale network structure (Figure 1c, 2a, S2e). So, the anisotropic structuring of the DRIB films network can be described by affine deformation and, this deformation is important for the formation of the discs, but *how is the anisotropy of the network translated into the anisotropic morphology of the crystal discs?*

Model of Disc Formation. To answer this question, we analyzed the morphological evolution of the crystals formed within the DRIB films as a function of time. NanoCT analysis allowed the size and 3D shape of a statistically-relevant number of crystals grown within the gels to be quantitatively analyzed. This analysis revealed that the shape of the crystals evolved from spheres at 1 day to discs at 4 weeks (Figures 4a and S3a-l), which is reminiscent of crack growth evolution in soft materials.[47-49] According to linear-elastic fracture mechanics (LEFM), a "penny-shaped" crack will form in a soft solid if the process zone (area of damage around the crack tip) is smaller than the area of the crack[49] and when the internal pressure $P \sim \sqrt{\Gamma E / l}$, where Γ is the work to fracture, E is the modulus of a soft solid, and l is the length of the crack.[48] The internal pressure can also be expressed as $P \sim Ew/l$ where w is the width of the crack.[47] Equating the two expressions for P, a simple crack growth model (SCGM) is obtained $l/w \sim \sqrt{l/(\Gamma/E)}$.[49] This model predicts that a crack in a soft solid will grow with an aspect ratio that depends on the ratio between w and the elasto-adhesive length, Γ/E, of the solid. In our case, the SCGM generally describes the shape evolution of the crystals obtained from the nanoCT analysis (Figure 4a), indicating that the growing crystals fracture the network and are "molded" by these fractures into discs. Based on this fitting, Γ/E of the DRIB films can be estimated as 10.0 ± 0.2 μm. Inversely, we can measure the mechanical properties of DRIB gels and use those measurements to estimate Γ/E. The DRIB gels exhibit anisotropic mechanical properties having higher moduli, E, and requiring higher work to fracture, Γ, parallel versus perpendicular to the drying direction (Figures 4b and S7). Using the measured values for DRIB gels, Γ/E can be estimated as 24.4 ± 5.4 μm, where E is 1.20 ± 0.17 MPa measured parallel and Γ is 29.2 ± 5.0 J m^{-2} measured perpendicular to the drying direction of the films.

Based on these findings, we propose the following explanation for how the calcite discs form in the affinely deformed DRIB films. Diffusion of calcium and carbonate ions into the DRIB film results in crystal nucleation and growth. As crystals grow, they exert a crystallization pressure, P_{cryst}, on their surroundings, which can be expressed as:[43] $P_{\mathrm{cryst}} \sim \frac{RT}{v_{\mathrm{m}}} \ln(\sigma)$ where R is the gas constant, T is the temperature (in Kelvin), v_{m}

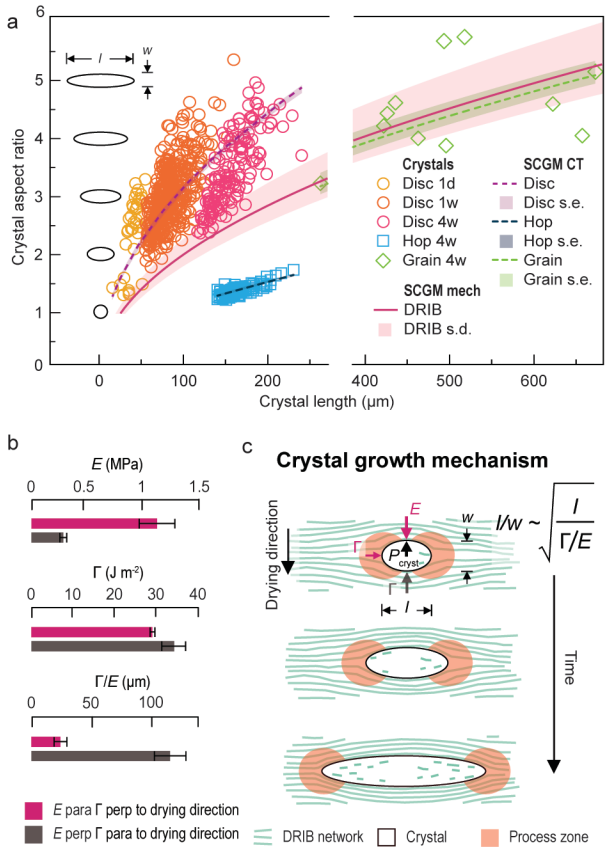

Figure 4. a) A plot showing the relationship between crystal aspect ratio, l/w, and length, l. The circular symbols represent measurements made via nano-computer tomography (nanoCT) analysis of the discs formed in a dried-rehydrated Agarose IB (3 w/v%, DRIB) film after 1 day, 1 and 4 weeks, the square symbols represent the hoppers formed in a dried-rehydrated Agarose IX gel (3 w/v%, DRIX) film after 4 weeks and the diamond symbols represent the rice-grain-shaped crystals formed in a DRIB cylinder after 4 weeks, diffusion (50 mM $CaCl_2$ and $NaHCO_3$). According to linear elastic fracture mechanics (LEFM), a simple crack growth model (SCGM; equation in(c)) can be used to describe the elongation of a crack in a neo-Hookean solid with an aspect ratio, l/w, which depends on the ratio between the crack length, l, and the elasto-adhesive length, Γ/E, of the solid, where Γ is the work to fracture and E is the modulus of the solid.[49] The SCGM CT dashed lines are fit using the SCGM and the length, l, and aspect ratio, l/w, of the crystals measured using the nanoCT data, and the shaded areas flanking these lines is the standard error (s.e.). The SCGM mech solid line is fit using the SCGM and the Γ/E of the DRIB film, and the shaded area flanking this line is the standard deviation (s.d.). b) Graphs showing the measured E, Γ, and Γ/E of the DRIB films. Violet bars: E measured parallel and Γ perpendicular to the drying direction, and the Γ/E of these two. Gray bars: E measured perpendicular and Γ parallel to the drying direction, and the Γ/E of these two. The data represented by the violet bars' is that used to plot the SCGM mech line in (a). c) A schematic of the proposed mechanisms by which the calcite discs form in the DRIB films. LEFM typically works well for specimens and crack sizes that are bigger than the process zone (area of damage around the crack tip).

is the molar volume of the solid phase, and σ is the supersaturation of the solution. The P_{cryst} exerted by the calcite crystals in the DRIB films can then be estimated as ~8.5 MPa. The P_{cryst} exerted by the crystals may also become anisotropic. As the crystals fracture the network, solution will flood into the fractures, increasing the relative ion concentration (i.e., σ) and hence P_{cryst} in the direction of the fractures. If a counter-pressure greater than P_{cryst} is exerted on the face of the crystal, the crystal cannot grow. Note that, in our system, P_{cryst} is comparable to the elastic modulus of the gel, so that stresses exerted by the gel on the crystal should be strong enough to hinder crystal growth. The easiest route for the crystals to grow is then by fracturing open the network in the direction perpendicular to the drying plane where the fracture resistance is the least (as measured, Figure 4b). Thus, the crystals fracture the gel parallel to the drying plane, resulting in the growth of discs "molded" by the shape of the fractures (Figure 1g, 3a-c, 4a,c, S3i-l, S5, S6g-l). In addition to the anisotropic mechanical environment the growing crystals encounter, the ionic concentration gradients surrounding the crystals may also become anisotropic as the gel fractures, further promoting the anisotropic growth of the crystals into discs.

As the discs form, they likely maintain the crystallographic orientation, with respect to the gel network, established at nucleation (Figure S6) and occlude those parts of the network that are strong enough to resist the P_{cryst} exerted by the crystals,[22,25] forming into composites (Figure 3e, S5a,b). Given that the discs occlude part of the network, they require less work to fracture their way through it, which is reflected in the different Γ/E values obtained from the nanoCT versus the mechanical testing data (Figure 4a, "SCGM mech" compared to "SCGM CT"). Using the measured modulus, E, of the gel, the work to fracture, Γ, during growth can be estimated as 12.0 ± 1.7 J m^{-2}. The crystals formed in the anisotropically structured, overall weaker, DRIX films (Figure 1d), experience lower counter pressure and fracture resistance in all directions, forming into isotropic hopper-like crystals. Also, the DRIX gel is likely too weak to be occluded and is excluded from the growing crystals (Figures 3j and S5c,d), consistent with previous reports of calcite growth in agarose IX gels.[22,25]

Extending to 2D Deformation. If our interpretation of the results is correct, we should be able to control calcite crystal formation in an agarose gel that is anisotropically-structured in 2D, not just one-dimension (1D). To test this idea, we dried and rehydrated agarose gel cylinders, which resulted in them maintaining their length and radially contracting (Figure 5a and S8). Precipitation of calcium carbonate in the cylinders resulted in rice-grain-shaped crystals, with the long-axis of the crystals running parallel to the central axis of the cylinders (Figure 5b-d). The grains display the characteristic{104} facets of calcite (Figure 5h), however, there is no apparent preferred crystallographic orientation with respect to the long-axis of the grains. The SCGM model broadly describes the shape of the rice-grain crystals formed in the cylinders (Figure 4a), indicating that the grains also form due to fracture. As the crystals grow in the cylinders, they likely experience lower counter pressure and fracture resistance parallel to the long-axis of the cylinder, which is perpendicular to the radial drying direction and so fracture their way through the gel network in this direction forming into the observed rice-grain morphologies.

Broader Applicability. Using calcite and agarose as a representative model crystal-gel pair, we have demonstrated how anisotropic, yet compliant gel networks can be used to fabricate crystal composites with predictable anisotropic forms. We envisage that this approach can be extended to use a variety of different types of gels. For example, gels with tunable anisotropic mechano-structural properties,[50] would enable finer

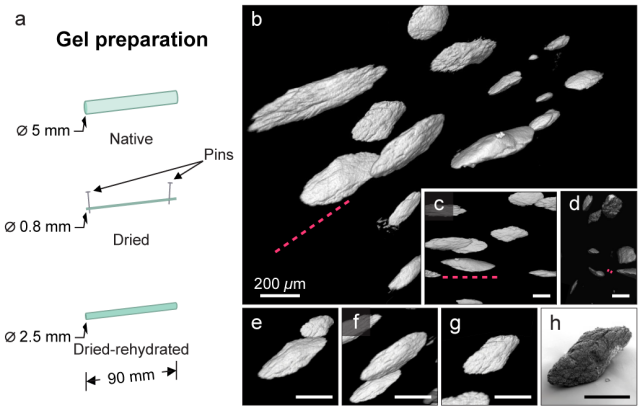

Figure 5. a) A schematic illustration of the drying-rehydration approach used to structure the agarose gel cylinders. b-g) Images generated from reconstructed nano-CT data of crystals formed in a dried-rehydrated Agarose IB gel (3 w/v%; DRIB) cylinder after 4 weeks diffusion (50 mM $CaCl_2$ and $NaHCO_3$). b) Overview, c) side and d) end view images of the crystals, and e-g) isometric images of individual crystals. h) SEM image of an individual crystal. The pink dashed line in (b,c,d) runs parallel to the central axis of the cylinder. All scale bars are 200 μm.

mechanical control over crystal-shape anisotropy, whereas gels with tailored chemical functionalities,[29,31-33] could afford chemical control over crystal shape, crystallographic orientation, and texture. We also envisage that this approach can be extended to add direction-specific functionality (e.g., mechanical, optical, electronic, or magnetic properties) into the resulting composites by using gels doped with functional nanoparticles,[36,37,39] crystals with intrinsic functional properties,[38,40,41] or both, resulting in advanced anisotropically-structured crystal composites for applications such as repair of mineralized tissues,[51] cementitious materials construction,[52] energy storage and conversion,[53] and photonics.[54]

CONCLUSION

We have developed a novel, biologically-inspired approach for forming anisotropic crystal composites within structured gels. Precipitation of calcium carbonate in anisotropically-structured agarose gel films and cylinders resulted in the formation of agarose-calcite composite discs and rice-grain shaped crystals, respectively. The formation of these composites can be explained by the mechanical occlusion of the gel[22,25] and fracture formation within the gel network. As such, this work adds to our understanding of Nature's mechanical use of organic frameworks to modulate her mineralized tissues. It also provides a promising platform for rationally fabricating anisotropically-structured polymer-reinforced crystalline materials with direction-specific and emergent functional properties for a broad range of applications.

MATERIALS AND METHODS

Gel Preparation and Structuring. Gels were produced from Agaroses Type IB and Type IX (Sigma-Aldrich). Gel solutions were prepared by dissolving agarose powder (3 w/v%) in hot deionized (DI) water (18.2 MΩ cm^{-1}, Barnstead Easypure RoDI). Native agarose films and cylinders were formed by pouring the solutions into polystyrene Petri dishes (100 × 20 mm) and silicone tubing (internal Ø 5 mm), respectively. The NIB gel films and cylinders were allowed to cool in the Petri dishes and tubes at room temperature, and the NIX gel films were cooled in the Petri dishes in a refrigerator (8ºC ± 2ºC) for 30 min. The NIB and NIX films were dried in the Petri dishes, and the NIB cylinders were removed from the tubes, pinned at points 90 mm apart, and dried in air overnight. The DIB and DIX films and DIB cylinders were rehydrated in DI water (~100 mL) for 30 min resulting in DRIB and DRIX films and DRIB cylinders.

Calcite Crystal Growth. Crystal growth in the gel films and fibers was achieved by the solution-based double diffusion of $CaCl_2$•$2H_2O$ (50 mM, ≥99%, Sigma-Aldrich, in DI water) and $NaHCO_3$ (50 mM, ≥99%, Sigma-Aldrich, in DI water) at room temperature for up to 4 weeks. The diffusion setup for the gel films consisted of an internal reservoir (2 L, 50 mM $CaCl_2$•$2H_2O$) and an external reservoir (3 L, 50 mM $NaHCO_3$), separated by a gel film fitted and sealed with adhesive (RTV108, Momentive Performance Materials Inc.) to an aperture (Ø 60 mm) in the base of the internal reservoir. The setup for the gel cylinders consisted of two reservoirs (1 L, 50 mM $CaCl_2$•$2H_2O$ and 1 L, 50 mM $NaHCO_3$) connected by a silicone tube (internal Ø 5 mm) containing a length (~90 mm) of gel cylinder fitted and sealed with adhesive. The solutions for the cylinder experiments were replenished after 2 weeks. At the end of each diffusion experiment, the gels were removed from the setups and rinsed in DI water.

Gel Characterization. We examined the swelling behavior of the agarose films and cylinders by stereomicroscopy (Leica L2). To do so, we took images of the cross-sections of native agarose IB (NIB), dried agarose IB (DRIB) and dried rehydrated agarose IB (DRIB) films and cylinders, and native agarose IX (NIX), dried agarose IX (DIX) and dried-rehydrated (DRIX) films. The sections were prepared by cutting the gels with a new/sharp scalpel blade parallel to the drying plane. The sections were then clamped in self-closing tweezers with their cross-sections facing up towards the microscope objective for imaging. Hydrated samples were kept in DI water until the moment of imaging.

Scanning Electron Microscopy. The network structure of the NIB, DRIB, and DRIX gel films were imaged via scanning electron microscopy (SEM, Zeiss Gemini 500). Before imaging, the gel films were fixed using glutaraldehyde (2 w/v%) in sodium cacodylate buffer (0.05 M) for 2 hours at 4ºC. The gels were rinsed in 0.05 cacodylate buffer 3 times, soaking for 5-10 min each time. They were dehydrated in a graded series of ethanol solutions: 50%, 70%, 95% and 100%, 10 min each, and then 100% for 3 days. The gels were then placed in the chamber of a critical point drier; the chamber was flushed ~3 times with liquid CO_2 and gels left to soak in liquid CO_2 for a minimum of 2 days at ~5ºC. The critically point dried films were cryogenically fractured between two tweezers after being held in liquid nitrogen for 5 min. The fracturing was made to expose the cross-sections through the drying plane of the films. The samples were mounted on carbon tape with their cross-sections facing upwards and sputter coated with Au/Pd at 30 mA for 20 seconds. Images were taken of the cross-sections utilizing an InLense detector at an accelerating voltage of 1.00 kV and a working distance of ~2.5 mm. To determine for network orientation, fast Fourier transforms of the images were produced using MATLAB R2018b (MathWorks).

X-ray Diffraction. Two-dimensional X-ray diffraction (2D-XRD) patterns of the NIB, DIB, and DRIB gel films were collected on a general area detector diffraction system

(GADDS, Bruker D8) using Cu Kα radiation (1.54 Å). The films (~50 mm^2) were mounted on an aluminum stage using Kapton tape such that the incident beam was approximately parallel (at a grazing angle 2.2°) and then remounted such that it was perpendicular to the drying plane of the films, and so that the films were ~9 cm from the detector. Azimuthal line profiles and radial sectors of selected 2D-XRD patterns were integrated using the Nika package for Igor Pro 6 (Wavemetrics).[55] Azimuthal line profiles were collected for the DIB films centered at 1.4 $Å^{-1}$, the DRIB films centered at 1.0 $Å^{-1}$, and for the NIB films centered at 0.8 $Å^{-1}$, with widths of ~0.5 $Å^{-1}$. For integrated sector averages (integration along q), data was processed for all the same peaks using a sector width of 10˚.

Mechanical testing. The modulus, E, and fracture energy, Γ, of the DRIB films were measured. E was measured via the unconfined compression of gel cubes (~40 mm^3) using a dynamic mechanical analyzer (DMA Q800, TA Instruments) and estimated as the slope of the initial linear region of the stress-strain curve. Stress was measured as force per unit area of the initial cross-section of the cubes and strain as $E = (h-h_0)/h_0$ where h_0 is the initial height of the cube, and h is the height during compression. Γ was measured via a T-peel test (ASTM D1876-08) on gel strips (4 × 10 × 90 mm) using a tensile testing stage (TST350, Linkam Scientific Instruments) and calculated as $\Gamma = 2F/w$, where F is the average applied steady-state force, and w is the width of the gel strip.[56] The cubes and strips were prepared by casting films with a final thickness of 4 mm. A custom-made tool consisting of two new/sharp blades mounted parallel to each other was then used with one action to cut out strips from the films and then cubes from the strips. The gel strips for the T-peel test were mounted on cotton fabric with extra thick cyanoacrylate adhesive (BSI-135H, Bob Smith Industries Inc.). Gel cubes and mounted strips were kept in DI water until the moment of testing.

Crystal Characterization. Crystals formed in the gels were examined by plane-polarized light microscopy (Leica DM EP) to determine their morphology and distribution within the gels and through cross-polarizers to determine their single-crystal-like character. Crystals were gently picked out from the gels with an 18-gauge syringe needle while viewed using a light microscope. Some of the crystals were etched in DI water for 4 days, and both unetched and etched crystals were carefully placed on silicon wafers sputter-coated with Au/Pd and imaged via SEM as above.

Raman Spectroscopy. Raman spectra were obtained for the crystals formed in the DRIB and DRIX films and for geological calcite (Iceland spar, Ward's Scientific) by confocal Raman microscopy (Renishaw InVia, equipped with a RenCam CCD detector) through a 50× long-working-distance objective (Leica Microsystems). Spectra were acquired with a 488 nm laser for 10 s at 10 mW, over a range of 100-1600 cm^{-1} and with a resolution of 1 cm^{-1}, and were the average of 10 scans.

NanoCT. NanoCT (Zeiss/Xradia Versa XRM-520) scans were taken to analyze the morphology of crystals formed in the dried-rehydrated gel films. Five gel discs (10 mm diameter) were punched out from each film using a biopsy punch, stacked together, and placed in a microcentrifuge tube. A drop (500 μL) of DI water was added to the tube before sealing with parafilm to prevent dehydration of the gel discs. Scans were made for each gel stack at 60 kV, and 5 W. Tomographic data was reconstructed using Zeiss reconstruction software (XM Reconstructor) and binned to a final resolution of 0.7-5 μm/pixel. Analysis of the data was performed in Aviso Fire. Crystals were segmented from the gel based on the difference in their density using the threshold tool. The crystal volumes were rendered, and their length, width, and volume were measured using the measurement tool. Crystals were excluded from the data sets if their volume was <400 μm^3 and if the borders of the scan volumes intersected them.

Modeling. The azimuthal intensity profiles generated from the 2D scattering images taken parallel to the film were fitted to the modified affine deformation model[44] using Origin Pro (Origin Lab). The goodness of fit for MADM models was determined using Efron's pseudo-R2.[57] The nanoCT data (aspect ratio and length) of the crystals were fitted to the simple crack growth model[49] using the Nonlinear Least Squares method using R 3.5.2 (The R Foundation).

ASSOCIATED CONTENT

Supporting Information

The Supporting Information (Figures S1-S8) is available free of charge on the ACS Publication website at

Supplementary figures.

AUTHOR INFORMATION

Corresponding Author

***Lara A. Estroff** – *Department of Materials Science and Engineering, Cornell University, Ithaca, NY 14853, USA; Kavli Institute at Cornell for Nanoscale Science, Ithaca, NY 14853, USA;* orcid.org/0000-0002-7658-1265; E-mail: lae37@cornell.edu

Authors

Damian Palin – *Department of Materials Science and Engineering, Cornell University, Ithaca, NY 14853, USA; Materials & Environment section, Department 3MD Faculty of Civil and Engineering and Geosciences Delft University of Technology 2628 CN Delft, The Netherlands*

Robert W. Style – *Laboratory of Soft and Living Materials Department of Materials, ETH Zurich, 8093 Zurich, Switzerland.*

Jure Zlopaša – *Department of Biotechnology, Faculty of Applied Sciences, Delft University of Technology, 2629 HZ Delft, The Netherlands*

Jonathan J. Petrozzini – *Department of Materials Science and Engineering, Cornell University, Ithaca, NY 14853, USA.*

Mark A. Pfeifer – *Cornell Center for Materials Research Cornell University, Ithaca, NY 14853, USA*

Henk M. Jonkers – *Materials & Environment section, Department 3MD, Faculty of Civil Engineering and Geosciences, Delft University of Technology, 2628 CN Delft, The Netherlands*

Eric R. Dufresne – *Laboratory of Soft and Living Materials, Department of Materials, ETH Zurich, 8093 Zurich, Switzerland*

Notes

The authors declare no competing financial interests.

ACKNOWLEDGMENT

This project has received funding from the European Union's Framework Horizon 2020 research and innovation programme

under the Marie Sklodowska- Curie Grant Agreement No.747736. It also made use of the Cornell Center for Materials Research (CCMR) Shared Facilities, supported through the NSF MRSEC program (DMR-1719875), and received partial support came from the U. S. Department of Energy (DOE), Basic Energy Sciences (BES) under award DE-SC0010560. NanoCT Imaging data was acquired through the Cornell Institute of Biotechnology's Imaging Facility, with NIH 1S10OD012287 funding for the Zeiss-Xradia Versa 520 X-ray microscope. The authors would like to thank Philip Carubia, Malcolm Thomas, and John Grazul in the CCMR, Teresa Porri, in the Cornell Biotechnology Resource Center-Imaging facility, for their support in collecting the data, and Zach Rouse in the Department of Materials Science and Engineering, Cornell University, and Yu Mo in the School of Geography and The Environment, University of Oxford, for the helpful discussions.

REFERENCES

(1) Wegst, U. G.; Bai, H.; Saiz, E.; Tomsia, A. P.; Ritchie, R. O., Bioinspired structural materials. *Nat. Mater.* **2015**, 14 (1), 23-36.

(2) Amini, S.; Tadayon, M.; Idapalapati, S.; Miserez, A., The role of quasi-plasticity in the extreme contact damage tolerance of the stomatopod dactyl club. *Nat. Mater.* **2015**, 14 (9), 943-950.

(3) Ling, S.; Kaplan, D. L.; Buehler, M. J., Nanofibrils in nature and materials engineering. *Nature Rev. Mater.* **2018**, 3 (4), 1-15.

(4) Huang, W.; Restrepo, D.; Jung, J. Y.; Su, F. Y.; Liu, Z.; Ritchie, R. O.; McKittrick, J.; Zavattieri, P.; Kisailus, D., Multiscale toughening mechanisms in biological materials and bioinspired designs. *Adv. Mater.* **2019**, 31 (43), 1901561.

(5) Polishchuk, I.; Bracha, A. A.; Bloch, L.; Levy, D.; Kozachkevich, S.; Etinger-Geller, Y.; Kauffmann, Y.; Burghammer, M.; Giacobbe, C.; Villanova, J.; Hendler, G.; Sun, C.-Y.; Giuffre, A. J.; Marcus, M. A.; Kundanati, L.; Zalansky, P.; Pugno, N. M.; Gilbert, P. U. P. A.; Katsman, A.; Pokroy, B., Coherently aligned nanoparticles within a biogenic single crystal: a biological prestressing strategy. *Science* **2017**, 358 (6368), 1294-1298.

(6) DeRocher, K. A.; Smeets, P. J.; Goodge, B. H.; Zachman, M. J.; Balachandran, P. V.; Stegbauer, L.; Cohen, M. J.; Gordon, L. M.; Rondinelli, J. M.; Kourkoutis, L. F.; Joester, D., Chemical gradients in human enamel crystallites. *Nature* **2020**, 583 (7814), 66-71.

(7) Xu, Y.; Nudelman, F.; Eren, E. D.; Wirix, M. J.; Cantaert, B.; Nijhuis, W. H.; Hermida-Merino, D.; Portale, G.; Bomans, P. H.; Ottmann, C., Intermolecular channels direct crystal orientation in mineralized collagen. *Nat. Commun.* **2020**, 11 (1), 1-12.

(8) Gim, J.; Schnitzer, N.; Otter, L. M.; Cui, Y.; Motreuil, S.; Marin, F.; Wolf, S. E.; Jacob, D. E.; Misra, A.; Hovden, R., Nanoscale deformation mechanics reveal resilience in nacre of Pinna nobilis shell. *Nat. Commun.* **2019**, 10 (1), 1-8.

(9) Aizenberg, J.; Sundar, V. C.; Yablon, A. D.; Weaver, J. C.; Chen, G., Biological glass fibers: correlation between optical and structural properties. *Proc. Natl. Acad. Sci.* **2004**, 101 (10), 3358-3363.

(10) Li, L.; Kolle, S.; Weaver, J. C.; Ortiz, C.; Aizenberg, J.; Kolle, M., A highly conspicuous mineralized composite photonic architecture in the translucent shell of the blue-rayed limpet. *Nat. Commun.* **2015**, 6 (1), 1-11.

(11) Harting, P., On the artificial production of some of the principal organic calcareous formations. *J. Microsc. Sci.* **1872**, 20, 118-23.

(12) Leduc, S., La biologie synthétique. A. Poinat: **1912**; Vol. 2.

(13) Miles, F., The apparent hemihedrism of crystals of lead chloride and some other salts. *Proc. R. Soc. London, A* **1931**, 132 (819), 266-281.

(14) Berman, A.; Addadi, L.; Weiner, S., Interactions of sea-urchin skeleton macromolecules with growing calcite crystals—a study of intracrystalline proteins. *Nature* **1988**, 331 (6156), 546-548.

(15) Orme, C. A.; Noy, A.; Wierzbicki, A.; McBride, M. T.; Grantham, M.; Teng, H. H.; Dove, P. M.; DeYoreo, J. J., Formation of chiral morphologies through selective binding of amino acids to calcite surface steps. *Nature* **2001**, 411 (6839), 775-779.

(16) Heywood, B. R.; Mann, S., Template-directed nucleation and growth of inorganic materials. *Adv. Mater.* **1994**, 6 (1), 9-20.

(17) Aizenberg, J.; Black, A. J.; Whitesides, G. M., Controlling local disorder in self-assembled monolayers by patterning the topography of their metallic supports. *Nature* **1998**, 394 (6696), 868-871.

(18) A. Berman, D. J. Ahn, A. Lio, M. Salmeron, A. Reichert, D. Charych, *Science* **199**5, 269, 515.

(19) Park, R. J.; Meldrum, F. C., Synthesis of single crystals of calcite with complex morphologies. *Adv. Mater.* **2002**, 14 (16), 1167-1169.

(20) Finnemore, A. S.; Scherer, M. R. J.; Langford, R.; Mahajan, S.; Ludwigs, S.; Meldrum, F. C.; Steiner, U., Nanostructured calcite single crystals with gyroid morphologies. Adv. Mater. **2009**, 21 (38-39), 3928-3932.

(21) Ha, J.-M.; Wolf, J. H.; Hillmyer, M. A.; Ward, M. D., Polymorph selectivity under nanoscopic confinement. *J. Am. Chem. Soc.* **2004**, 126 (11), 3382-3383.

(22) Asenath-Smith, E.; Li, H.; Keene, E. C.; Seh, Z. W.; Estroff, L. A., Crystal growth of calcium carbonate in hydrogels as a model of biomineralization. *Adv. Funct. Mater.* **2012**, 22 (14), 2891-2914.

(23) Henisch, H. K., Crystal growth in gels. Courier Corporation: **1996**.

(24) McCauley, J. W.; Roy, R., Controlled nucleation and crystal growth of various CaC03 phases by the silica gel technique. *Am. Min: J. Earth Plan. Mater.* **1974**, 59 (9-10), 947-963.

(25) Li, H.; Estroff, L. A., Calcite Growth in Hydrogels: Assessing the Mechanism of Polymer-Network Incorporation into Single Crystals. *Adv. Mater.* **2009,** 21 (4), 470-473.

(26) Regitsky, A. U.; Keshavarz, B.; McKinley, G. H.; Holten-Andersen, N., Rheology as a Mechanoscopic Method to Monitor Mineralization in Hydrogels. *Biomacromolecules* **2017**, 18 (12), 4067-4074.

(27) Chernov, A., Modern Crystallography III, Springer Series in Solid-State Sciences. **1984**.

(28) Falini, G.; Fermani, S.; Gazzano, M.; Ripamonti, A., Biomimetic crystallization of calcium carbonate polymorphs by means of collagenous matrices. *Chem.- Eur. j.* **1997**, 3 (11), 1807-1814.

(29) Nudelman, F.; Pieterse, K.; George, A.; Bomans, P. H. H.; Friedrich, H.; Brylka, L. J.; Hilbers, P. A. J.; de With, G.; Sommerdijk, N. A. J. M., The role of collagen in bone apatite formation in the presence of hydroxyapatite nucleation inhibitors. *Nat. Mater.* **2010**, 9 (12), 1004-1009.

(30) Li, H.; Estroff, L. A., Hydrogels coupled with self-assembled monolayers: an in vitro matrix to study calcite biomineralization. *J. Am. Chem. Soc.* **2007**, 129 (17), 5480-5483.

(31) Falini, G., Crystallization of calcium carbonates in biologically inspired collagenous matrices. *Int. J. Inorg. Mater.* **2000**, 2 (5), 455-461.

(32) Grassmann, O.; Müller, G.; Löbmann, P., Organic−inorganic hybrid structure of calcite crystalline assemblies grown in a gelatin hydrogel matrix: relevance to biomineralization. *Chem. Mat.* **2002**, 14 (11), 4530-4535.

(33) Fukao, K.; Nonoyama, T.; Kiyama, R.; Furusawa, K.; Kurokawa, T.; Nakajima, T.; Gong, J. P., Anisotropic Growth of Hydroxyapatite in Stretched Double Network Hydrogel. *ACS nano* **2017**.

(34) Gavira, J. A.; García-Ruiz, J. M., Agarose as crystallisation media for proteins II: trapping of gel fibres into the crystals. *Acta Crystallogr., Sect. D* **2002**, 58 (10), 1653-1656.

(35) Li, H.; Xin, H. L.; Muller, D. A.; Estroff, L. A., Visualizing the 3D internal structure of calcite single crystals grown in agarose hydrogels. *Science* **2009**, 326 (5957), 1244-1247.

(36) Kim, Y.-Y.; Schenk, A. S.; Walsh, D.; Kulak, A. N.; Cespedes, O.; Meldrum, F. C., Bio-inspired formation of functional calcite/metal oxide nanoparticle composites. *Nanoscale* **2014**, 6 (2), 852-859.

(37) Liu, Y.; Yuan, W.; Shi, Y.; Chen, X.; Wang, Y.; Chen, H.; Li, H., Functionalizing Single Crystals: Incorporation of Nanoparticles Inside Gel-Grown Calcite Crystals. *Angewandte Chemie* **2014**, 126 (16), 4211-4215.

(38) Asenath-Smith, E.; Hovden, R.; Kourkoutis, L. F.; Estroff, L. A., Hierarchically structured hematite architectures achieved by growth in a silica hydrogel. *J. Am. Chem. Soc.* **2015**, 137 (15), 5184-5192.

(39) Liu, Y.; Zang, H.; Wang, L.; Fu, W.; Yuan, W.; Wu, J.; Jin, X.; Han, J.; Wu, C.; Wang, Y.; Xin, H. L.; Chen, H.; Li, H., Nanoparticles incorporated inside single-crystals: enhanced fluorescent properties. *Chem. Mat.* **2016**, 28 (20), 7537-7543.

(40) Ren, J.; Niu, M.; Guo, X.; Liu, Y.; Yang, X.; Chen, M.; Hao, X.; Zhu, Y.; Chen, H.; Li, H., Bulk-heterojunction with long-range ordering: C60 single-crystal with incorporated conjugated polymer networks. *J. Am. Chem. Soc.* **2020**, 142 (3), 1630-1635.

(41) Kim, S.; Regitsky, A. U.; Song, J.; Ilavsky, J.; McKinley, G. H.; Holten-Andersen, N., In situ mechanical reinforcement of polymer hydrogels via metal-coordinated crosslink mineralization. *Nat. Commun.* **2021**, 12 (1), 667.

(42) Correns, C. W., Growth and dissolution of crystals under linear pressure. *Discuss. Faraday Soc.* **1949**, 5, 267-271.

(43) Rijniers, L.; Huinink, H.; Pel, L.; Kopinga, K., Experimental evidence of crystallization pressure inside porous media. Phys. Rev. Lett. **2005**, 94 (7), 075503.

(44) Zlopasa, J.; Norder, B.; Koenders, E. A.; Picken, S. J., Origin of highly ordered sodium alginate/montmorillonite bionanocomposites. *Macromolecules* **2015**, 48 (4), 1204-1209.

(45) Foord, S.; Atkins, E., New x-ray diffraction results from agarose: Extended single helix structures and implications for gelation mechanism. *Biopolymers* **1989**, 28 (8), 1345-1365.

(46) Kuhn, W.; Grün, F., Beziehungen zwischen elastischen Konstanten und Dehnungsdoppelbrechung hochelastischer Stoffe. *Kolloid-Zeitschrift* **1942**, 101 (3), 248-271.

(47) Sneddon, I. N., The distribution of stress in the neighbourhood of a crack in an elastic solid. *Proc. R. Soc. London, A* **1946**, 187 (1009), 229-260.

(48) Lin, Y.-Y.; Hui, C.-Y., Cavity growth from crack-like defects in soft materials. *Int. J. Frac* **2004**, 126 (3), 205-221.

(49) Kim, J. Y.; Liu, Z.; Mook Weon, B.; Hui, C.-Y.; Dufresne, E. R.; Style, R. W., Scale-free fracture in soft solids. *Sci. Adv.* **2020**, 6, eaaz0418.

(50) Richtering, W.; Saunders, B. R., Gel architectures and their complexity. *Soft Matter* **2014**, 10 (21), 3695-3702.

(51) Place, E. S.; Evans, N. D.; Stevens, M. M., Complexity in biomaterials for tissue engineering. *Nat. Mater.* **2009**, 8 (6), 457-470.

(52) Bechthold, M.; Weaver, J. C., Materials science and architecture. *Nat. Rev. Mater.* **2017**, 2 (12), 1-19.

(53) Li, W.; Liu, J.; Zhao, D., Mesoporous materials for energy conversion and storage devices. *Nat. Rev. Mater.* **2016**, 1 (6), 1-17.

(54) Soukoulis, C. M.; Wegener, M., Past achievements and future challenges in the development of three-dimensional photonic metamaterials. *Nat. Photonics* **2011**, 5 (9), 523-530.

(55) Ilavsky, J., Nika: software for two-dimensional data reduction. *J. Appl. Crystallogr.* **2012**, 45 (2), 324-328.

(56) A. Gent, A. Kinloch, *J. Polym. Sci., Part A-2: Polym. Phys.* **1971**, 9, 659.

(57) Efron, B., Regression and ANOVA with zero-one data: Measures of residual variation. *J. Am. Stat. Assoc.* **1978**, 73 (361), 113-121.

“For Table of Contents Only” (8.26 cm × 3.4 cm).